Research in Astronomy and Astrophysics, 25:075020 (15pp), 2025 July

https://doi.org/10.1088/1674-4527/addbc7
CSTR: 32081.14.RAA.addbc7

The Overview and Trial Observations of AIMS

Yuanyong Deng[1,2], Dongguang Wang[1], Jianwen Hua[3], Songbo Xu[4], Ming Liang[5], Lianwei Zhao[3], Xianyong Bai[1,2,6], Zhiwei Feng[1,2], Guangqian Liu[7], Yuliang Shen[1], Biyuan Gao[1,2], Liyue Tong[1], Xiaoming Zhu[1], Wei Duan[1,2], Xingming Bao[1], Meng Mou[3], Zhanhu Wang[3], Yongqi Zhang[4], Shangjie Ren[4], Hua Li[4], Xing Fu[4], Yu Lei[4], Kewei E[4], Rong Gao[4], Yang Bai[1], Xiao Yang[1], Ziyao Hu[1], Junfeng Hou[1,2], Jiaben Lin[1], Yingzi Sun[1], Huili Che[1], Xing Hu[1], Yufei Feng[1], Zhekai Wang[1], Mingfu Shao[1,2], Wenxian Li[1,2], Yuyang Ye[1,2], Yuchuan Wu[1,2], Kaifan Ji[7], Hengyu Mu[7,2], Jianwei Xue[1], Jingyu Wang[1], Aimin Jiang[1], Baolin Tan[1,2], Quan Wang[1], Shangbing Yang[1,2], Jiangtao Su[1,2], Xiaofan Wang[1], Yongliang Song[1], Gang Xu[1], Jian Wang[1], Chensen Wang[1], and Zongtai Tang[1]

[1] State Key Laboratory of Solar Activity and Space Weather, National Astronomical Observatories, Chinese Academy of Sciences, Beijing 100101, China; dyy@nao.cas.cn, xybai@bao.ac.cn
[2] School of Astronomy and Space Science, University of Chinese Academy of Sciences, Beijing 100049, China
[3] Shanghai Institute of Technical Physics, Chinese Academy of Sciences, Shanghai 200080, China
[4] Xi'an Institute of Optics and Precision Mechanics, Chinese Academy of Sciences, Xi'an 710119, China
[5] National Optical-Infrared Astronomy Research Laboratory, Tucson, AZ 85726, USA
[6] Institute for Frontiers in Astronomy and Astrophysics, Beijing Normal University, Beijing 102206, China
[7] Yunnan Observatories, Chinese Academy of Sciences, Kunming 650216, China
Received 2025 March 24; revised 2025 May 1; accepted 2025 May 6; published 2025 June 24

Abstract

The infrared band contains rich opportunities for astronomical research, but due to the limitations of infrared technology, the development of infrared astronomy in China has been far from satisfactory for a long time, especially for solar observation. "Accurate Infrared Magnetic field Measurements of the Sun" project (AIMS) is a National Major Scientific Research Instrument Development Project (recommended by the Ministries) supported by the National Natural Science Foundation of China. It is aimed at improving the accuracy of magnetic field measurement by an order of magnitude, by measuring the "Zeeman splitting" directly. In addition, as AIMS is also the first equipment specifically designed for mid- to far-infrared solar observation in the world, we also hope to utilize AIMS to explore potential new scientific research opportunities in the vast infrared region. This article will briefly introduce the scientific objectives, the telescope, the scientific post-focus instruments, and finally summarize the commissioning observations of AIMS.

Key words: Sun: infrared – methods: observational – instrumentation: spectrographs

1. Introduction

A magnetic field plays an important role in understanding the mechanism of solar and stellar activities. In 1908, Hale (1908) first measured the solar magnetic field. From then on, solar and space physics made great progress in the broad aspects related to the solar magnetic field. Up to now, there are several ways to measure the solar magnetic field. However, the method applied by Hale based on the Zeeman effect is undoubtedly the most effective and broadly used.

The fundamental point of measuring magnetic fields using the Zeeman effect lies in the fact that in the solar atmosphere with a magnetic field, spectral lines undergo splitting. The separation between these split spectral sub-lines is proportional to the magnetic field strength, with a specific functional relationship given by:

$$\Delta\lambda_B = 4.67 \times 10^{-13} g \lambda^2 B, \quad (1)$$

Here, g is the effective magnetic sensitivity factor, e.g., Lande factor, λ is the central wavelength in Angstrom, $\Delta\lambda_B$ is the separation from the line center, and B is the strength of the magnetic field in Gauss. Moreover, these split spectral lines exhibit different polarization states.

For specific spectral lines, their Lande factor and wavelength are determined. So theoretically, once the Zeeman splitting distance is measured, the magnetic field strength can be determined. However, in the current routinely conducted magnetic field observations in the visible and near-infrared bands, the Zeeman splitting is very small compared to the width of solar spectral lines, making it difficult to measure the Zeeman splitting directly in most cases. An effective method is to exploit the different polarization states between Zeeman sub-lines by conducting polarization measurements and inverting these polarization profiles using the theory of polarized radiation transfer in the solar atmosphere to obtain information about the solar magnetic field (Unno 1956). Therefore, the current mature method for measuring solar magnetic fields essentially converts it into a measurement of polarization parameters of solar spectral lines. This is an "indirect measurement" method, and the measurement results strongly

depend on the radiation transfer model of the solar atmosphere. Unfortunately, determining the solar atmospheric model requires many physical parameters, which are often not directly accessible and can only be inferred based on the local solar atmospheric environment, with no guarantee of accuracy. This leads to issues such as non-uniqueness and limited precision in the inversion results (del Toro Iniesta & Cobo 2016). Furthermore, the magnetic field itself is an important parameter in the model, making the inversion process somewhat self-circular. Therefore, the dependence of existing magnetic field measurement methods on the solar atmospheric model is a significant drawback.

In addition, such methods introduce another drawback, namely that the sensitivity to transverse magnetic field components is much poorer than that to longitudinal components. Through some simple assumptions, J. Evans (1966) provided a simple estimate of the relationship between the sensitivity to longitudinal and transverse magnetic field components,

$$B_T \approx 70\sqrt{B_L}, \tag{2}$$

where B_T is the sensitivity to transverse components (components perpendicular to the line of sight) and B_L is the sensitivity to longitudinal components (components along the line of sight). Therefore, even though the current solar magnetic field telescopes can achieve longitudinal magnetic field measurement sensitivities up to several Gauss, the transverse field measurement sensitivity is only on the order of tens even hundreds of Gauss (Deng et al. 1999; Jin et al. 2009). This significantly limits the accurate measurement of magnetic field strength.

Because the Zeeman splitting is proportional to the square of the wavelength, while the width of solar spectral lines is generally proportional to the first power of the wavelength, the Zeeman effect-induced splitting of spectral lines becomes much more pronounced relative to the line width in the mid- and far-infrared bands due to the large wavelength values in these regions. Brault & Noyes (1983) pointed out that, under the same Lande factor, the Zeeman splitting in mid-infrared spectral lines is more than two orders of magnitude higher than that in the visible light region. The relative width of the Zeeman splitting to the spectral line is also more than 25 times higher than that of visible light under the same conditions. Therefore, the mid-infrared band offers the potential for directly measuring the Zeeman splitting. This can transform the traditional "indirect measurement" of magnetic fields back into a "direct measurement," thereby improving the accuracy of magnetic field measurements and reducing the dependence on solar atmospheric models. Consequently, this method will no longer rely on radiative transfer models. Moreover, by converting traditional polarization intensity measurements into polarization profile positioning measurements, the impact of instrumental polarization and crosstalk will be significantly reduced, thereby greatly improving the accuracy of magnetic field measurements.

Given the potential advantages of mid and far-infrared (IR) observations, scientists began exploring the scientific value of infrared solar observations and their technical feasibility in the 1970s. The representative achievements were mainly experimental observations conducted at the Mg I 12.32 μm using the McMath-Pierce Solar Telescope, which was the largest solar optical telescope at that time. These studies included those by Hewagama et al. (1993) and Moran et al. (2000), who used a BIB (Blocked Impurity-Band) detector in combination with an FTIR (Fourier transform infrared spectrometer) to obtain complete Stokes parameters in 7 minutes for a point source. Additionally, Jennings et al. (2002) and Moran et al. (2007) used a BIB 128 × 128 array detector with a grating spectrometer, achieving a spectral resolution of approximately 0.6 nm and completing Stokes spectroscopic measurements of line sources within 5 min. These pioneering works demonstrated the feasibility and advantages of measurements of the magnetic field in mid and far-IR. However, since these efforts were conducted using experimental equipment, they did not form a systematic scientific observation and research framework. In recent years, with the implementation of infrared scientific terminals on the Goode Solar Telescope (GST), the GREGOR telescope, and the Daniel K. Inouye Solar Telescope (DKIST), infrared observations have seen significant development (Schmidt et al. 2012; Rimmele et al. 2020; Yang et al. 2020). DKIST is currently equipped with two infrared terminals: the Diffraction-Limited Near-Infrared Spectro-Polarimeter (DL-NIRSP) and the Cryogenic Near-Infrared Spectro-Polarimeter (CRYO-NIRSP). Schad et al. (2024) reported on coronal magnetic field observations using CRYO-NIRSP. The Cryogenic Infrared Spectrograph (CYRA) on GST focuses on solar spectral observations between 1 and 5 μm and has been conducting observations for several years (Yang et al. 2020). Judge et al. (2024) used the GREGOR Infrared Spectrometer (GRIS) to analyze magnetic field changes from the photosphere to the upper chromosphere. It is evident that although infrared solar observations have made substantial progress in recent years, infrared magnetic field measurements have primarily been conducted in the near and mid-infrared below 5 μm, failing to fully leverage the advantage of "direct measurement" of solar magnetic fields in the mid and far-infrared.

"Accurate Infrared Magnetic field Measurements of the Sun" project, hereafter AIMS, was proposed based on the aforementioned scientific ideas. The project was supported by the National Natural Science Foundation of China in 2014 December through the National Major Scientific Research Instrument Development Project (recommended by the Ministries), and was officially launched in 2016 May. It has now completed all the development work and has been installed at the Saishiteng Mountain in Lenghu, Qinghai Province, where it began scientific trial observations in 2023 September.

In this paper, we will briefly introduce the scientific objectives, the telescope, and the scientific post-focus instruments of AIMS in Section 2. In Section 3, we will demonstrate the scientific observation capabilities of AIMS through the

Table 1
Main Performance and Design Parameters of AIMS

Telescope effective aperture	1 m
Observation spectral line	Mg I 12.32 μm
Designed Field of View	$192'' \times 192''$
Spectral resolving power	0.004 cm^{-1}
Detector array	64×2
Spatial resolution	$1.''5$ $pixel^{-1}$
FTIR temporal resolution	30 s
Magnetic field measurement accuracy	10G
Wide-band imaging system	
Operating wavelength range	8–10 μm
Field of view	Φ $384''$
Detector array	256×256
Spatial resolution	$1.''5$ pixel
Temporal resolution	20 ms

data obtained during the commissioning observations. Section 4 will be dedicated to the summary and discussion.

2. Overview of AIMS

2.1. Scientific Objectives and Top-level Design Requirements

2.1.1. Scientific Objectives

The core scientific objective of AIMS is to establish a mid-infrared measurement system and conduct astronomical observations, thereby breaking through the bottleneck issues that have persisted in solar magnetic field measurements for a century: the reliance on solar atmospheric models in the process of inverting polarization measurements to magnetic fields, and the significantly lower measurement accuracy of transverse components compared to longitudinal components. AIMS aims to improve the current measurement accuracy of the strength of solar magnetic fields by approximately an order of magnitude, achieving a measurement precision of 10 Gauss. Through more precise and quantitative observational data on solar magnetic fields, AIMS expects to achieve groundbreaking research results in solar physics.

2.1.2. Top-level Design Requirements around Scientific Objectives

To achieve the goal of directly measuring the Zeeman splitting, appropriate mid-infrared solar spectral lines should be selected, and the split spectral profiles should be obtained using a spectrograph. By determining the line center positions of the split sub-lines, the Zeeman splitting of the spectral lines can be obtained, thereby allowing the solar magnetic field strength information to be directly derived using the Zeeman splitting formula.There are significantly fewer magnetically sensitive spectral lines available for magnetic field measurements in the mid-to-far-infrared compared to the visible light region. The Mg I 12.3 μm line, which forms in the solar "temperature minimum zone," has a Lande factor of 1. Hewagama et al. (1993) successfully observed its triplet spectral lines using this line at the McMath-Pierce Solar Telescope at Kitt Peak. Therefore, AIMS has also selected it as its operating wavelength.

Obtaining the magnetic field strength directly by measuring the Zeeman splitting requires high spectral resolution, which poses a significant technical challenge for an infrared spectrograph. Therefore, it is necessary to determine appropriate specifications to achieve an optimal balance between scientific objectives and engineering feasibility. We conducted a simulation analysis based on the characteristics of the Mg I 12.32 μm spectral line and ultimately determined the spectral resolution specification for AIMS to be 0.004 cm^{-1}, which can achieve a measurement accuracy of 10 Gauss.

In the mid-infrared band, Fourier Transform Infrared Spectrograph (FTIR) is almost the only option to achieve such high spectral resolution, with a spectral resolving power of approximately 0.004 cm^{-1} (corresponding to 0.06 nm @ 12.32 μm). Therefore, the core scientific instrument of AIMS is the FTIR and its matching high-performance infrared detector. At the same time, considering the needs of imaging observations for solar physics research, we require the FTIR to have large field of view imaging capability, which is a user requirement that none of the international FTIR suppliers have encountered before, and thus becomes a major technical challenge and innovation point in the development of this project.

It is currently challenging to achieve a large array of high-performance infrared detector that matches the FTIR, so the project proposes a 64×2 line array detector. Under the constraint of the line array detector, in order to guide the FTIR in selecting and positioning observation targets, as well as to facilitate joint analysis and research with other equipment data, AIMS has also designed an 8–10 μm mid-infrared imaging system to complement the observations of FTIR. Main performance and design parameters of AIMS are shown in Table 1.

2.2. Telescope

2.2.1. Optical Design of the Telescope

AIMS adopts a classic off-axis Gregorian system, featuring a primary mirror (M1) with a clear aperture of 1 m and an off-axis distance of 1 m. The optical design is shown in Figure 1. A field stop with a diameter of Φ $6.'4$ is placed at the focus of the primary mirror. Mirrors M3–M6 constitute a Coudé system. M4 serves as an ellipsoidal relay mirror, extending the Gregorian focus to the desired position (intermediate focus). Mirror M6 reflects the chief ray and directs it vertically toward the Coudé room, aligning with the horizontal mechanical rotation axis. A derotator system is positioned in front of the intermediate focus. M7 is an off-axis parabolic mirror that converts the light from the intermediate focus into collimated light for subsequent focal plane instruments and

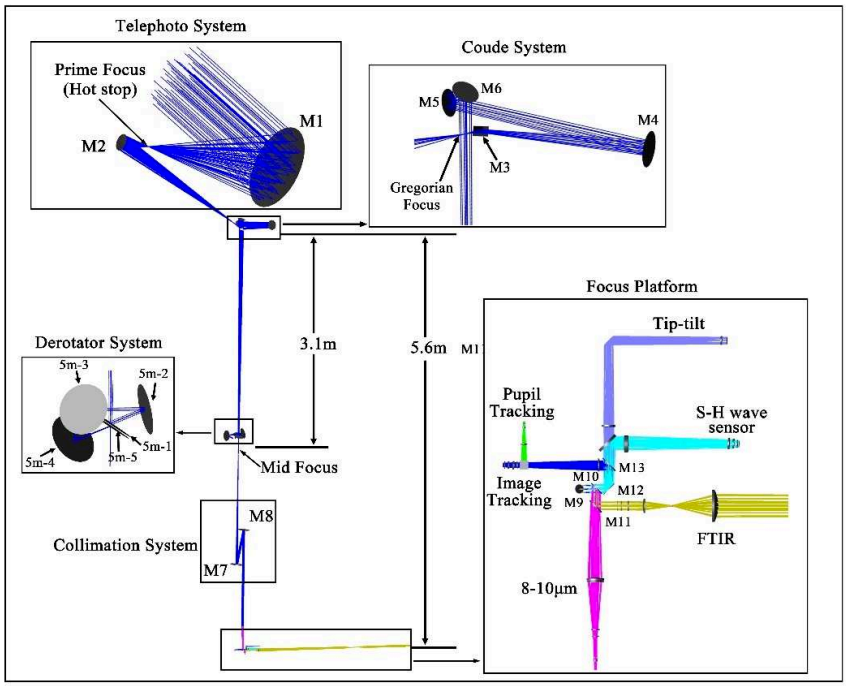

Figure 1. The optical design of AIMS.

detection optics. Mirror M8 is used for folding the optical path, while the 45° mirror M9 is located at the pupil position and is replaced by a tip-tilt mirror, also serving as a folding mirror. M10 reflects the light in the 12.32 μm and 8–10 μm wave bands and transmits light in other wave bands.

A polarization analyzer is placed in the collimated beam of the 12.32 μm optical path, and then the beam is converged by a lens to serve as the interface for the FTIR. Cold optics are positioned between the FTIR and the detector, where the cold stop of the telescope system is formed, thereby eliminating stray light outside the field of view. The M11 beamsplitter reflects the 8–10 μm beam for wide-band imaging, while light of other wavelengths is transmitted. The visible light, after being reflected by M11 and split by M12, is divided into two channels: the 550 ± 5 nm wavelength light is used for image tracking and pupil tracking, while the 630 ± 5 nm wavelength light is utilized for tip-tilt mirror monitoring and wave front detection.

The key specifications for the AIMS optical system are as follows (Table 2):

Table 2
Key Specifications for the AIMS Optical System

Effective Aperture	1 m
Off-Axis Distance	1 m
System Focal Ratio	$F/10$
Field of View	Φ 6.4
Operating Wavelength	0.5–12.5 μm
Spectral Resolution	0.004 cm^{-1} @ 12.32 μm
Tracking Accuracy (Without Tip-Tilt Mirror)	1″ per 30 minutes

Figure 2 presents the imaging quality test results of the center field for AIMS's each focus at –10°C, all of which meet the system design requirements.

2.2.2. Mechanical Design of the Telescope

The AIMS telescope structure primarily consists of the primary and secondary mirror mount assembly, a two-dimensional tracking turntable assembly, the support structure for the intermediate folded optical system, and the post-optical system structure within the Coudé room.

The main structure of the AIMS telescope (located in the Dome section, shown in Figure 3) primarily adopts a truss or steel plate welding design, with a total weight of approximately 15T (including counterweights). The outer envelope dimensions of the structure are 4268 mm × 2960 mm × 5788 mm, and the rotational contour diameter is Φ 5557 mm. The surface accuracy of the primary mirror of the telescope (shown in Figure 4), as measured on-site at 20°C, is better than $1/40\ \lambda$ @ 632.8 nm.

A fully absorbing thermal aperture is installed at the focus of the primary mirror, with an aperture of Φ 4.25 mm. The design of the hot stop is shown in Figure 5. The thermal aperture is cooled and temperature-controlled using a coolant, with the temperature maintained within a difference of less than 5°C from the ambient environment to minimize the impact on seeing caused by local temperature differences at the primary mirror focus.

The secondary mirror is precisely adjusted using a PI 6-axis hexapod (Shen et al. 2022), with adjustment accuracies of

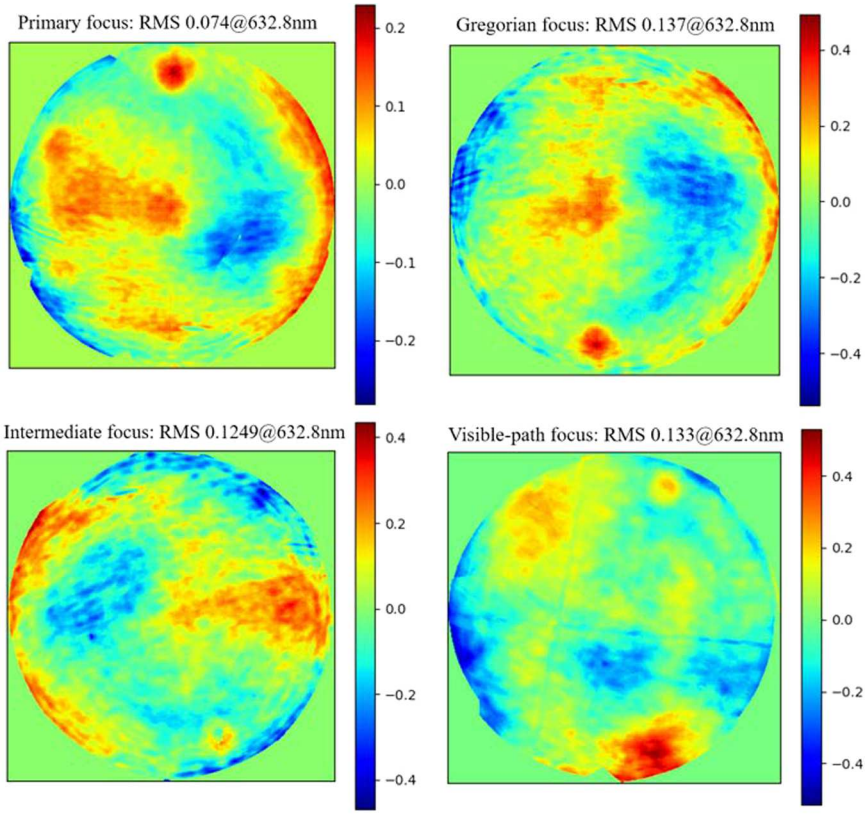

Figure 2. Tested imaging quality of center field for AIMS's each focus (–10°C).

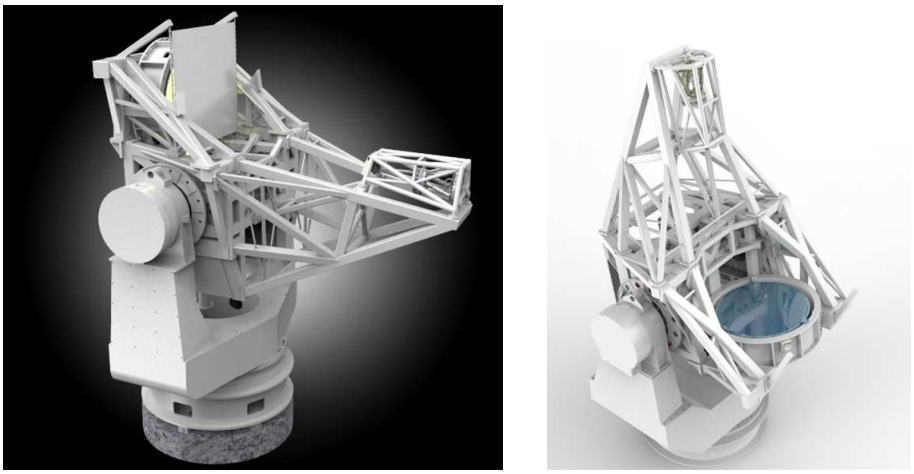

Figure 3. The main structure of AIMS.

2 μm for translation and 5 μrad for tilt. The use of the six-rod mechanism facilitates real-time correction of positional errors caused by temperature and attitude changes in the primary and secondary mirror mounts. In order to obtain the Look-up Table (LUT) of the 6-axis hexapod at different pitch angles, we developed a point source Shack-Hartmann wave front sensor. Based on nighttime measurement data, we found that the relative positioning errors between M1 and M2 at different pitch angles are primarily tilts in the horizontal and azimuthal directions. Therefore, we construct LUT for the alignment amounts of tilts in the horizontal and azimuthal at different pitch angles (24°–71°), as shown in Table 3. During daytime

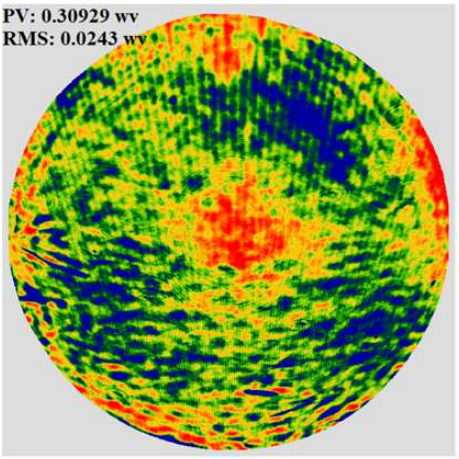

Figure 4. The surface accuracy of the primary mirror measured on-site at 20°C.

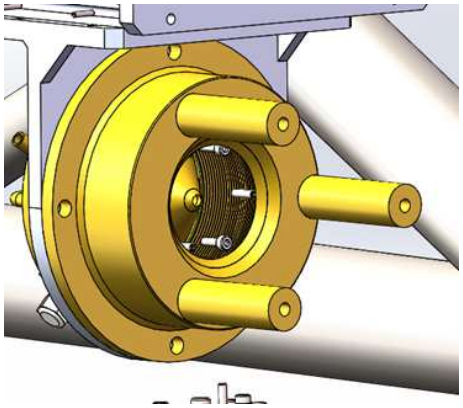

Figure 5. The design of the hot stop.

Table 3
The LUT of 6-axis Hexapod

Pitch Angle/°	Tilt in the Horizontal /°	Tilt in the Azimuthal /°
24	1.1418	0.1907
40	1.1503	0.1904
51	1.1468	0.1955
69	1.1317	0.1851
71	1.1433	0.1924

observations, the position of M2 is adjusted based on the LUT for different pitch angles to ensure the imaging quality of AIMS. The measured data indicates that the LUT of 6-axis hexapod significantly improved the image quality. The method has proven to be effective and practical. The measured data will be presented in Section 3.3.

The telescope achieves precise tracking through a two-dimensional tracking turntable, with the AIMS telescope

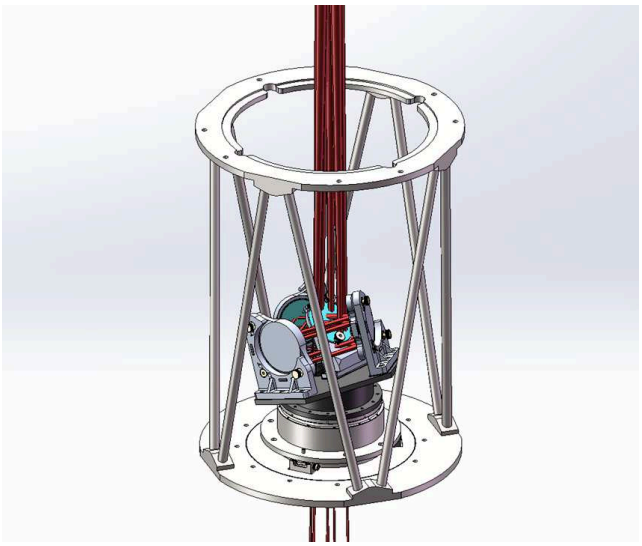

Figure 6. Five-mirror derotator system of AIMS.

achieving pointing and tracking accuracies of $5\farcs91$ (rms) and $0\farcs76$ (rms@30 minutes), respectively. Additionally, it is worth mentioning that the AIMS telescope adopts a five-mirror derotation structure (shown in Figure 6) to greatly reduce the impact of polarization (Hou et al. 2018). However, this complex structure presents new challenges for assembly and adjustment. We achieved a co-axiality error of $\pm10\farcs53$ between the incident optical axis and the mechanical rotation axis of the derotation mechanism using two laser theodolites, a pentaprism, and other tools. The specific assembly method can be found in reference (Lei et al. 2023).

2.2.3. The Tracking Control of the Telescope

The AIMS pointing and tracking control system (shown in Figure 7) is designed as a distributed, modular control system, with each module functioning relatively independently and integrated using Ethernet and fieldbus configuration. Based on functional structure, the system is divided into eight functional sub-blocks, with the core modules comprising the azimuth axis servo control system, elevation axis servo drive system, derotation servo control system, and full-disk opto-electronic guiding system. To ensure the system's safety, openness, controllability, and ease of expansion and maintenance, a safety and logic interlock system, a remote control interface and operation and maintenance database system, an operating environment and telescope status monitoring system, and a strong/weak electricity distribution system have been designed. The servo systems for the azimuth, elevation, and derotation axes have high real-time requirements, so separate controllers are used. Meanwhile, the full-disk opto-electronic guiding system, entrance pupil image monitoring system, and PLC status monitoring and logic control system, due to their lower real-time requirements and for ease of operation, are

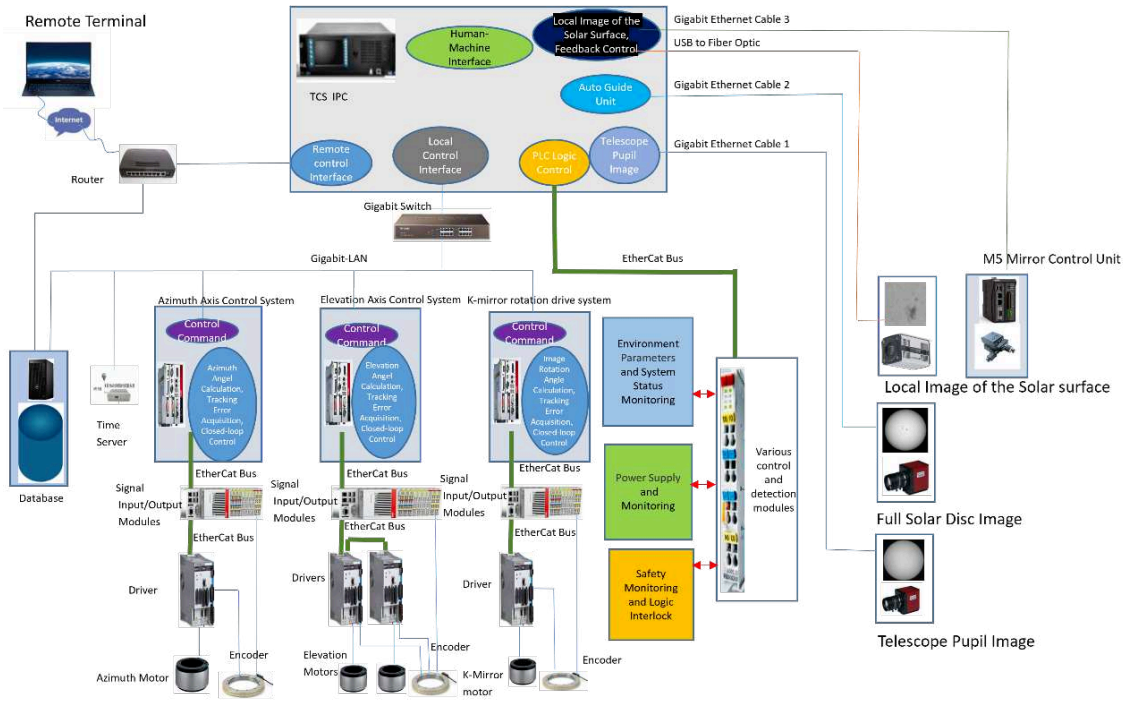

Figure 7. Telescope Control System.

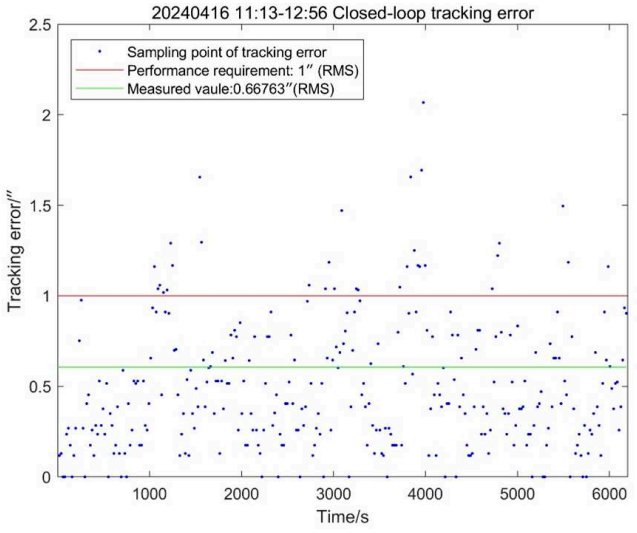

Figure 8. The closed-loop tracking test error of AIMS.

integrated into the central control computer platform. The closed-loop tracking test error of AIMS is shown in Figure 8, meeting the design specification requirement of better than 1″.

2.3. Scientific Instruments

Currently, AIMS is primarily equipped with a 12.32 μm FTIR system and an 8–10 μm wide-band imaging system. In the future, the possibility of extending a visible light observation system in the imaging tracking optical path can be considered.

2.3.1. FTIR (Infrared Fourier Transform Spectrograph)

The working principle of AIMS/FTIR is shown in Figure 9. The infrared radiation from the target enters the interferometer from the front, then passes through the subsequent optics, which maps the detected infrared radiation from the target onto the detector. The light signal received by the detector is the infrared radiation signal modulated by interference, referred to as the interference signal. The interference signal is processed through a Fourier transform to obtain the spectral signal of the radiation.

In design, the FTIR can be configured to observe with five different bandwidths: 12.32 ± 0.05 μm, 12.32 ± 0.1 μm, 12.32 ± 0.2 μm, 10–11 μm, and 10–13 μm. The spectral resolution is better than 0.004 cm^{-1} (FWHM) @12.32, which corresponds to a requirement for an optical path difference of at least 250 cm. The optical path difference is generated by the movement of the interferometer's moving mirror. The FTIR interferometer has a quadruple-pass structure, with a theoretical moving mirror travel distance of at least 62.5 cm.

The FTIR employs a 128-element Mercury Cadmium Telluride (HgCdTe) detector. Because the spectral detection in the central field of view is more effective than in the edge field of view, observation effects are better closer to the optical axis. Thus, the 128-element detector is arranged in a 64×2 format, i.e., 2 columns with 64 elements in each column, as shown in Figure 10.

Table 4
The Tested Spectral Resolution in Typical Units

Pixel Number	1	2	63	64	127	128
Spectral resolution	0.0037 cm^{-1}	0.0038 cm^{-1}	0.0037 cm^{-1}	0.0037 cm^{-1}	0.0039 cm^{-1}	0.004 cm^{-1}

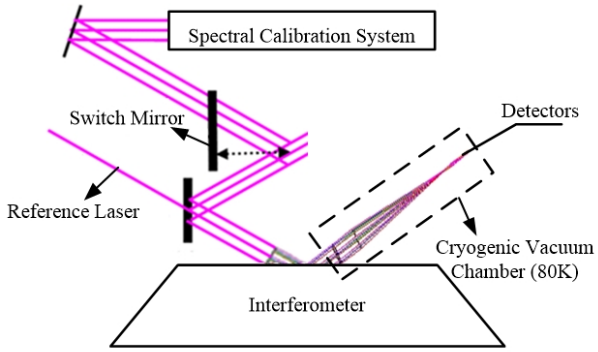

Figure 9. The principle of AIMS/FTIR.

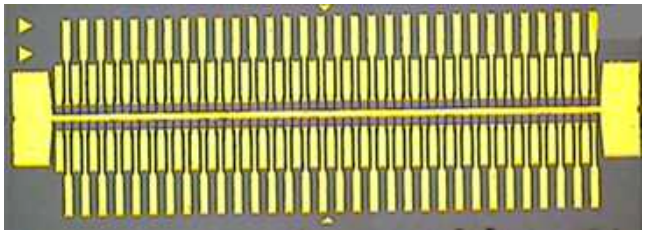

Figure 10. The diagram of the detector layout.

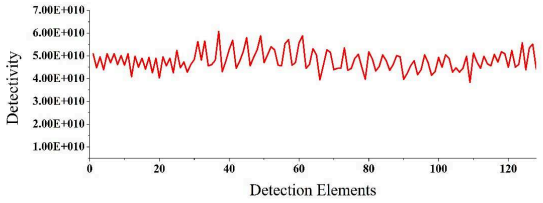

Figure 11. The tested detectivity of each detector unit.

The measured detectivity of each detection unit of the FTIR is better than 4×10^{10}, as shown in the test results (Figure 11). The spectral resolution of a typical unit is presented in Table 4, with all indicators meeting or exceeding the design values.

2.3.2. 8–10 μm Wide-band Imaging System

The 8–10 μm Wide-band Imaging System is primarily designed for solar imaging monitoring. Its main objective is to obtain evolutionary information about solar atmospheric activities in the mid-infrared band, which is of great significance for studying the evolution mechanisms of white-light flares and other phenomena in this spectral range.

The 8–10 μm Wide-band Imaging System consists of three primary components: an optical system, a vacuum refrigeration system, and a data acquisition and control system for the detector (Wang et al. 2022; Feng et al. 2025). The overall sketch of the Mid-IR ITS is displayed in Figure 12. A 256×256 Mercury Cadmium Telluride (HgCdTe) focal plane array detector is employed with a pixel size of 30×30 μm. It is connected to the rear end of the AIMS telescope, offering a field of view of $\Phi\, 6\farcm4$ with a pixel resolution of $1\farcs5\ \mathrm{pixel}^{-1}$. The system is equipped with multiple narrowband filters, which can be switched according to observational requirements to select different wavelength bands and bandwidths for imaging. Table 5 lists the main performance and key parameters.

2.4. The Site

AIMS is placed in Saishiteng Mountain, Qinghai, China (as shown in Figure 13). Since 2018, we have installed a weather station, a spectrometer for precipitable water vapor) and solar equivalent of a Differential Image Motion Monitor (S-DIM), and carried out observations on weather elements, precipitable water vapor, and daytime seeing conditions for more than one year at this site. The median value of daytime precipitable water vapor is 5.25 mm for the whole year, and it is 2.1 mm in winter seasons. The median value of the Fried parameter of daytime seeing is 3.42 cm. Its solar direct radiation data shows that the solar average observable time is 446 minutes per day in 2019 August. The details about the site survey can be found in Bao et al. (2023).

3. Commissioning Observations

AIMS began trial observations on 2023 August 31, and as of 2024 October 20, it has observed for a total of 149 days, generating 24.7 TB of raw data. Among these, FTIR observations were conducted for 120 days, producing 23.1 TB of raw data, while the 8–10 μm imager observed for 119 days, yielding 1.57 TB of raw data. Through more than a year of trial observations, the observation modes and calibration methods for the two focal plane scientific terminals have been established and integrated into the AIMS observation control system, enabling automatic observations. Below are some of the trial observation results.

3.1. Accuracy of Magnetic Field Measurement

AIMS has achieved solar spectral observations using a line-source FTIR for the first time in the world, significantly enhancing the observational efficiency of FTIR. Figure 14

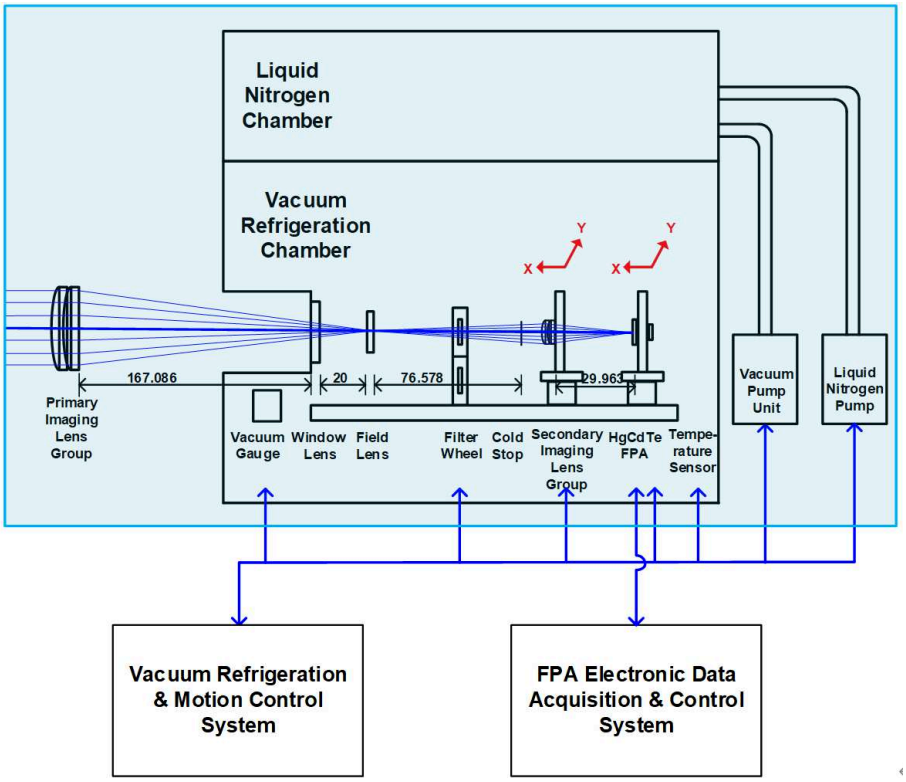

Figure 12. Block diagram of the 8–10 μm Wide-band Imaging System.

Table 5
Main Performance and Parameters of the 8–10 μm Wide-band Imaging System

Working Wavelength Band	8–10 μm
Field of View	Φ 384″
HgCdTe Infrared Focal Plane Array (IRFPA)	256 × 256, 30 μm × 30 μm pixel^{-1}
Temporal Resolution	20 ms
Working Temperature	$\leqslant$80 K
Filter Width (FWHM)	8.5 ± 0.085 μm; FWHM 0.50 ± 0.05 9.0 ± 0.09 μm; FWHM 0.50 ± 0.05
Observing Mode	Routine mode, Dark calibration mode, Flat field calibration mode

presents the spectral image of Mg I 12.32 μm taken by the 128-element detector of AIMS/FTIR. The observation and processing workflow for the spectral image primarily includes: The FTIR obtains a set of 128-element interferograms every 30 s, with 16 measurements conducted in total, taking 480 s. The spectral inversion for each of the 128 elements in the observed interferograms is performed using the method proposed by Bai et al. (2021) and Bai et al. (2023). There is inhomogeneity among the inverted spectra of different pixels. By utilizing the quiet region at the center of the solar disk and employing a random jittering method of the telescope, different flat field calibration matrices are obtained and applied for flat field correction. After flat field correction, spectral drifts still exist among different pixels, which are corrected using atmospheric spectral lines near Mg I 12.32 μm.

Figure 14 (upper) clearly shows the triple-split feature of the sunspot penumbra, demonstrating the advantage of the high magnetic field sensitivity of Mg I 12.32 μm. The emission intensity of Mg I at 12.32 μm is relatively weak in the umbra, which is consistent with the observations made by Bruls et al. (1994) using a point source Fourier Transform Infrared spectrometer. Figure 14 (bottom) presents the inverted spectrum of the 40th element, and the Zeeman splitting distance of the Mg I 12.32 μm line is obtained using a triple-Gaussian fitting method. The magnetic field strength is calculated based on the Zeeman splitting formula, with the standard deviation (1σ) of the fitting serving as the measurement accuracy of the magnetic field. The fitting result is shown as the solid black line, with a fitted magnetic field strength of 1346 G and a strength measurement error of 8.4 G.

Figure 13. A distant view of the AIMS tower and dome.

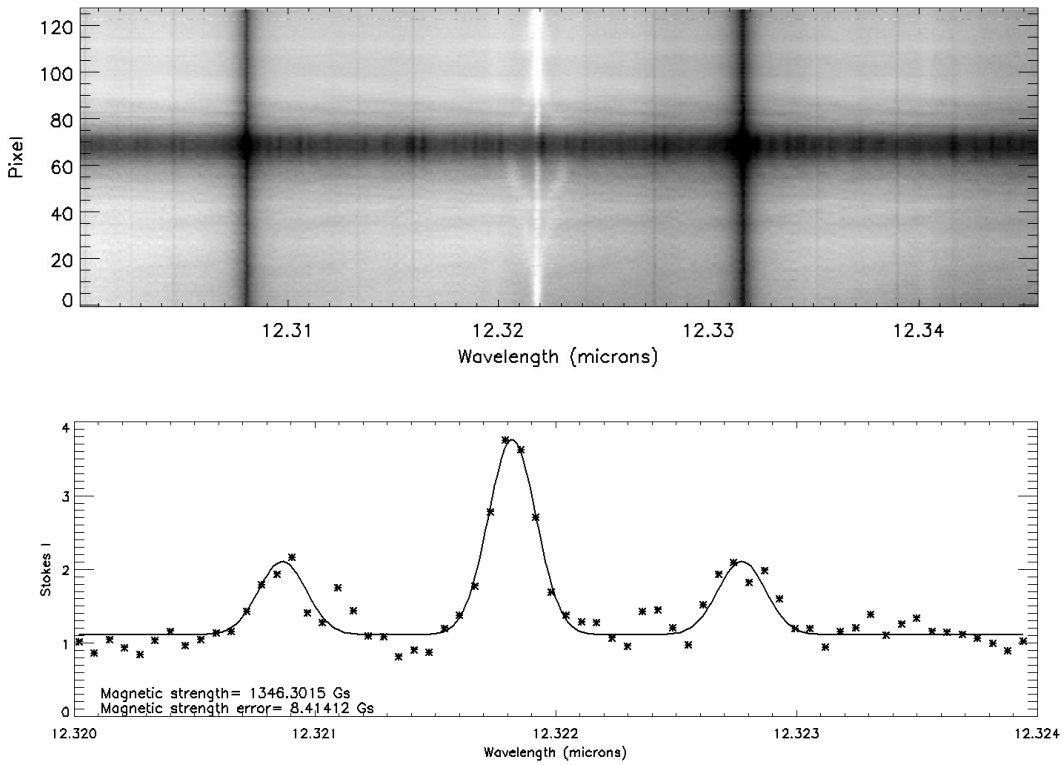

Figure 14. Observed spectrum of Mg I at 12.32 μm (top), and the spectral curve of the 40th element along with the total magnetic field strength fitted using a triple-Gaussian function (bottom).

In addition to measuring a 64×2-element spectrum in a single observation, AIMS can also cover a two-dimensional area of the solar surface through scanning observational mode. Figure 15 presents an intensity image of NOAA AR13796 obtained from a set of scans. The umbra and peumbra are distinctly identified.

3.2. Polarization Measurement

By means of measuring the Zeeman splitting, only the total magnetic field strength can be measured; the information on the inclination and azimuth of the magnetic field cannot be obtained. Thus, the polarized spectral observations are also

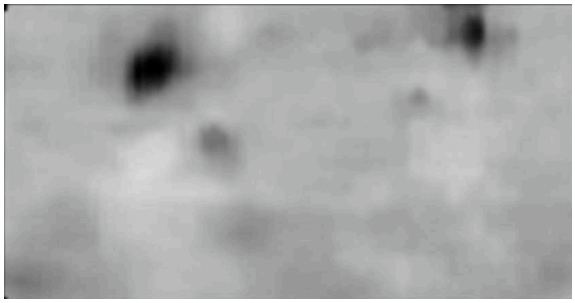

Figure 15. Scanned sunspot intensity of NOAA AR13796 on 2024 August 22.

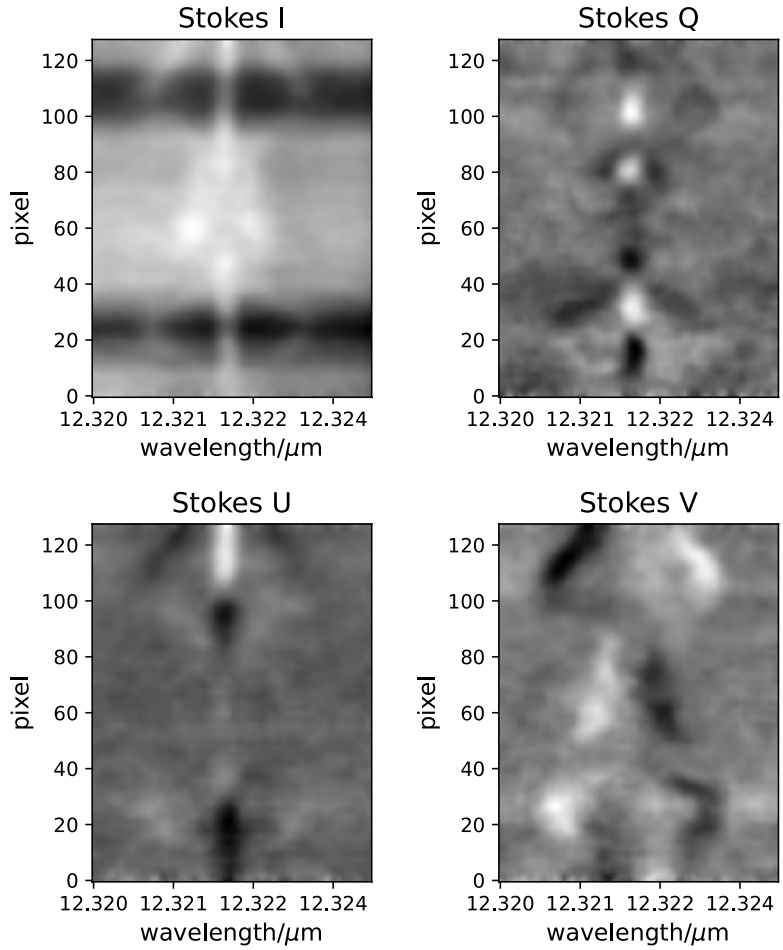

Figure 16. The Stokes *I*, *Q*, *U*, *V* polarized spectra of NOAA AR 13647 observed by AIMS.

necessary. In addition, polarized observations can provide magnetic field information in regions without triple splitting. Figure 16 presents a set of 128-element Stokes *I*, *Q*, *U*, *V* polarized spectral images observed on 2023 April 22. For Stokes *Q* and *U* linear polarization, axisymmetric spectral profiles can be observed, while for Stokes *V* circular polarization, centrally symmetric spectral profiles are visible, consistent with the spectral symmetry calculated by polarized radiation transfer theory.

The emission characteristics of the Mg I 12.32 μm line are caused by non-local thermodynamic equilibrium (NLTE) processes, which need to be considered in the inversion of

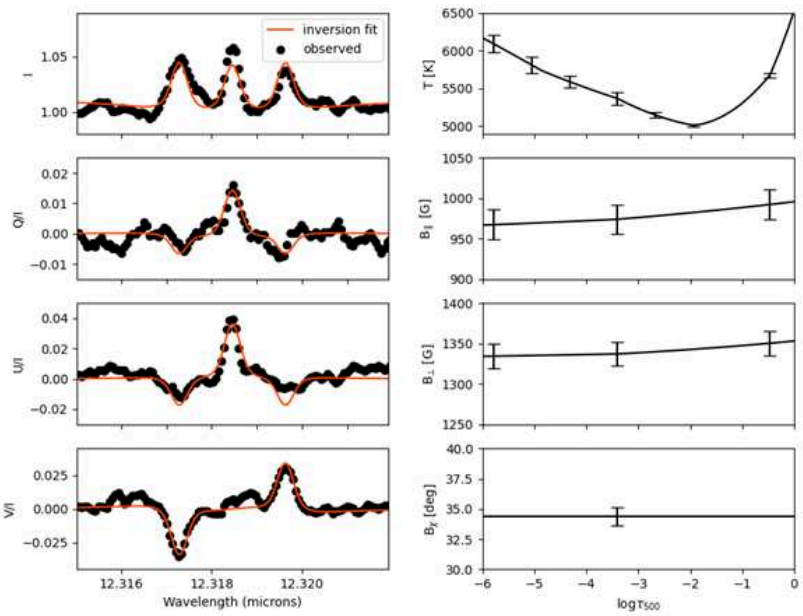

Figure 17. The NLTE inversion result for the 108-element in Figure 16. Left panel: The observed Stokes I, Q/I, U/I and V/I profiles (black circle) and inversion fitting (red curve) results for the penumbra region. Right panel: from top to bottom, the height distribution and errors of the inverted temperature (seven nodes), longitudinal magnetic field (three nodes), transversal magnetic field (three nodes), and magnetic field azimuth (one node).

polarized spectra. We used the STockholm inversion Code STiC NLTE inversion de la Cruz Rodríguez et al. (2019) to invert the polarized spectrum of the 108th element in Figure 17. The NLTE inversion can yield the temperature distribution as a function of height, as well as information on the total magnetic field strength, inclination, and azimuth.

3.3. Spatial Resolution in the Visible Wavelength

We also obtained some high-quality visible light images during the commissioning observations by the image tracking system. The quality of these visible light images is evaluated by Median Filter-Gradient Similarity (MFGS), which is used to screen the best image within sequences of short-exposure image tracking images. MFGS is a quality evaluation method for solar photosphere images that does not require a reference image. This method features monotonicity (value of the MFGS changes monotonically from 1 to 0 with degradation of image quality), linear correlation, and universality (Deng et al. 2015). From 2023 September to 2024 December, the image tracking system accumulated observations over 146 days. The MFGS value of the best single frame image is 0.746, with an average value of 0.49. Figure 18 shows observational samples of the image tracking system.

We collaborated with Yunnan Observatories to conduct high-resolution reconstruction based on the observational data from the image tracking system. Using NASIR (Non-rigid Alignment based Solar Image Reconstruction) (Liu et al. 2022), we performed image reconstruction to obtain high-resolution reconstructed images of the solar photosphere that approach the diffraction limit of AIMS (0.″14@550 nm). Figure 19 shows the high-resolution reconstructed image of NOAA AR 13719 on 2024 June 24, from image tracking system data, MFGS = 0.9955

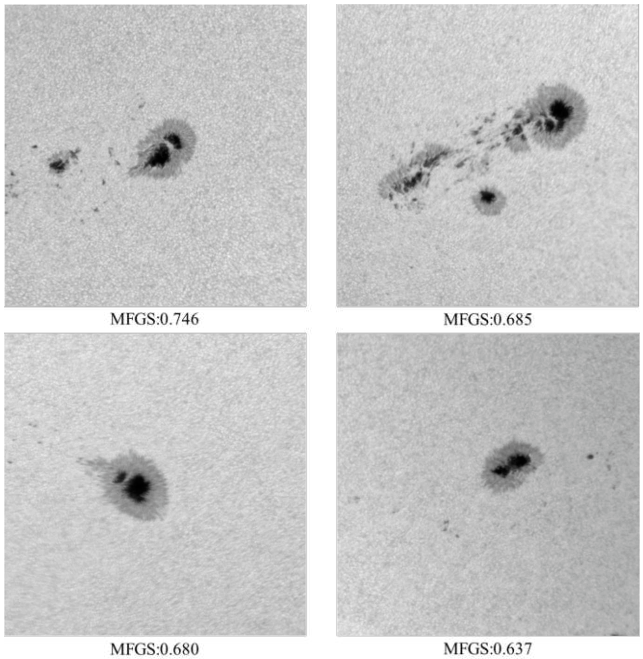

Figure 18. High spatial resolution samples obtained by the image tracking system.

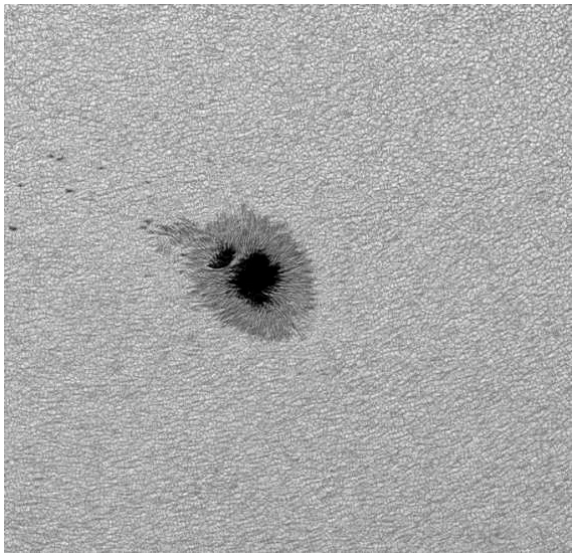

Figure 19. The high-resolution reconstructed image of NOAA AR 13719.

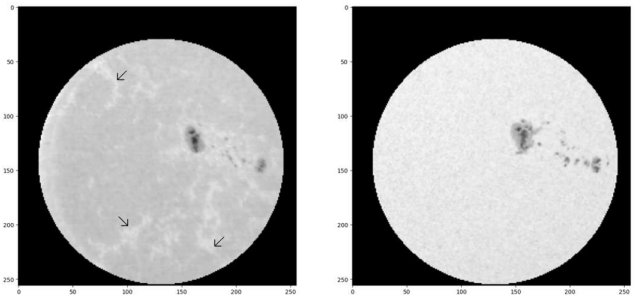

Figure 20. The observational data from the 8–10 μm wide-band imaging system taken on 2023 September 6 for NOAA AR 13421. Left: Image in 8–10 μm. Right: HMI intensity map observed in a similar time.

3.4. Wide-band Imaging in 8–10 μm

The 8–10 μm imaging system can capture the umbra and penumbra of sunspots in the mid-infrared band. Figure 20(a) presents a set of observations from this system, and Figure 20(b) shows observations from Helioseismic and Magnetic Imager (HMI) at a similar time. It can be observed that there are noticeable brightening structures in the regions surrounding the sunspot and corresponding to the network magnetic fields. Simões et al. (2017) pointed out that the formation height of the infrared continuum is higher than that of the visible continuum, providing information about the upper photosphere. This is the reason for the presence of brightening structures associated with network magnetic fields in the 8–10 μm observations. Furthermore, their simulation results also indicate that the formation height of the continuum can reach the chromosphere during flares. There have been previous examples of enhanced mid-infrared continuum radiation during flares (Penn et al. 2016). The pilot observation

Figure 21. Lunar crater captured by the 8–10 μm imager taken on 2024 August 18.

data from AIMS has captured multiple events of enhanced mid-infrared radiation during flares, providing data support for systematic studies of this phenomenon. Currently, the data processing software for the 8–10 μm imaging system has been developed, which mainly includes dark field and flat field calibration. We have also attempted to use the AIMS 8–10 μm imaging system for observations of non-solar targets. Figure 21 shows the features of a lunar crater captured on 2024 August 18. In the future, we will attempt to conduct mid-infrared observations of some bright stars.

4. Summary and Discussion

After nearly a decade of effort, AIMS has completed all its development work and has conducted a 15-month scientific pilot observation. The scientific observation results show that AIMS has achieved its core scientific goal, with a magnetic field measurement accuracy better than 10 Gauss. At the same time, AIMS can also perform rapid imaging observations in the 8–10 μm range.

The method of directly measuring the Zeeman splitting to obtain the magnetic field strength, although significantly improving measurement accuracy, still faces difficulties in separating Zeeman sub-lines when observing weak magnetic fields. That is, AIMS's direct measurement method still has limitations in its application scope. We have conducted simulation analyses on this (Li et al. 2021), and the results show that, without considering noise, AIMS's direct measurement method is effective for magnetic fields above 300 Gauss, meaning that it can resolve three components. The left panel of Figure 22 shows the results at transverse fields of 150, 300, and 450 G. Figure 22 shows an example of an actual observation, with a measured magnetic field strength of 440 Gauss, which is consistent with our simulation analysis. For weak magnetic fields below 300 Gauss, AIMS will revert to the traditional mode, using polarization measurements and inversion to obtain magnetic field information. As mentioned earlier, although the Zeeman splitting cannot be directly

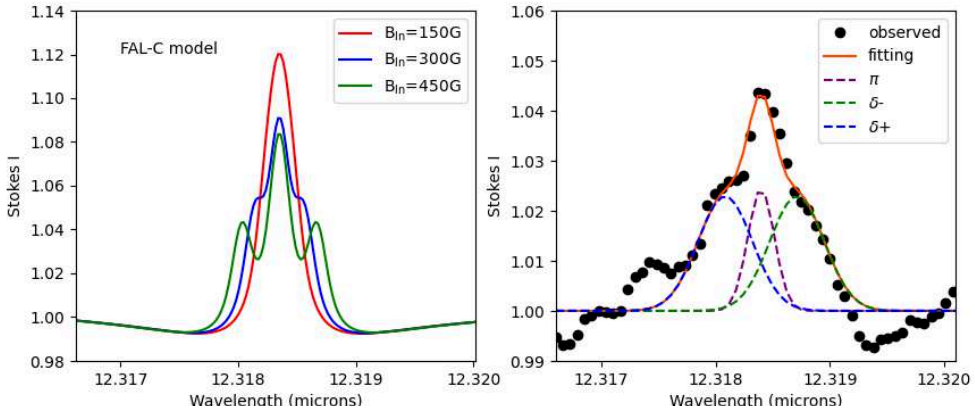

Figure 22. Lower limit of "direct measurement" by AIMS. Left: The forward simulation results show that splitting can be observed when the value exceeds 300G (Li et al. 2021). Right: An example of Stokes I of an AIMS observation (solid circle) and inversion fitting (red curve). The inversion results are in a longitudinal magnetic field of 256.5 G, transversal magnetic field of 362.1 G.

separated, the degree of splitting is still much greater than in the visible light range, thus significantly improving the measurement accuracy of weak magnetic fields.

Imaging is a very important observational capability for solar observations. Although AIMS is the first to achieve an imaging FTIR design internationally, and the measured spectral indicators all meet the imaging requirements, the current array detector cannot fully meet the high-performance needs of FTIR. Therefore, AIMS currently only uses a 64×2 line array device, which limits AIMS's full observational capabilities to some extent. In the future, we will continue to track technological advancements and seize the opportunity to replace the current detector system with a larger array detector.

In solar magnetic field measurements, both measurement accuracy and spatial resolution are very important indicators (Deng et al. 2009). Due to its long operating wavelength, AIMS has a lower spatial resolution in the operating band compared to other advanced equipment. Although this does not affect the achievement of AIMS's core scientific goals, it is still a slight imperfection. AIMS's optical design has taken this factor into account, so a visible light channel has been retained in the image tracking system of the Coudé room. In the future, we also consider upgrading this optical path and equipping it with the necessary high-resolution observational terminals to enhance AIMS's observational capabilities.

Polarization error plays a crucial and significant role in measurement accuracy. Theoretically, the additional polarization of a telescope is inversely proportional to the wavelength. Therefore, it is easier to achieve high-precision polarization measurements in the mid-infrared band than in the visible light band. In AIMS, we have significantly reduced the additional polarization of the telescope by adopting an unpolarized derotator design. The results of the systematic simulation show that the total instrumental polarization is below 0.003, and the polarization crosstalk is below 0.02, which is one to two orders of magnitude lower than that in the visible light band. Nevertheless, in the future, it is still necessary to conduct more systematic polarization calibration and crosstalk correction for the AIMS telescope, with the aim of obtaining polarization signals with higher sensitivity.

During the pilot observations, we conducted imaging observations of the Moon. In the future, we will also attempt to observe other celestial targets, such as observations of large planets like Jupiter, and spectral observations of some bright stars with strong magnetic fields.

Acknowledgments

AIMS is a National Major Scientific Research Instrument Development Project (recommended by the Ministries) supported by the NSFC under grant No. 11427901. We extend our sincere gratitude to the Qinghai Provincial Government departments at all levels, and particularly the Lenghu Industrial Park Administration Committee, for their invaluable support throughout the site selection and infrastructure construction of AIMS. We also appreciate Prof. Sen Wang, Dr. Zhiyong Zhang, Prof. Jie Jiang and Prof. Zhenyu Jin for their contributions in project planning and development.

References

Bai, X., Feng, Z., Zhang, Z., et al. 2023, RAA, 23, 125010
Bai, X.-Y., Zhang, Z.-Y., Feng, Z.-W., et al. 2021, RAA, 21, 267
Bao, X.-M., Wang, J., Jing, S., Deng, Y.-Y., & Wang, D.-G. 2023, RAA, 23, 115003
Brault, J., & Noyes, R. 1983, ApJL, 269, L61
Bruls, J., Solanki, K., Rutten, R., & Carlsson, M. 1995, A&A, 293, 225
de la Cruz Rodríguez, J., Leenaarts, J., Danilovic, S., & Uitenbroek, H. 2019, A&A, 623, A74
del Toro Iniesta, J. C., & Cobo, B. 2016, LRSP, 13, 4
Deng, H., Zhang, D., Wang, T., et al. 2015, SoPh, 290, 1479
Deng, Y., Wang, J., & Ai, G. 1999, ScChA, 42, 1096
Deng, Y., Wang, J., & Ai, G. 2009, AdSpR, 43, 365

Evans, D. S. 1966, in IAU Symp. 24, Spectral Classification and Multicolour Photometry, ed. K. Loden, L. O. Loden, & U. Sinnerstad (Cambridge: Cambridge Univ. Press), 342
Feng, Z., Zhang, Z. Y., Duan, W., et al. 2025, in press
Hale, G. E. 1908, ApJ, 28, 315
Hewagama, T., Deming, D., Jennings, D. E., et al. 1993, ApJS, 86, 313
Hou, J., Liang, M., Wang, D., & Deng, Y. 2018, OExpr, 26, 19356
Jennings, D. E., Deming, D., McCabe, G., Sada, P. V., & Moran, T. 2002, ApJ, 568, 1043
Jin, C., Wang, J., & Zhao, M. 2009, ApJ, 690, 279
Judge, P. G., Kleint, L., & Kuckein, C. 2024, ApJ, 970, 147
Lei, Y., Xu, S., Cao, M., et al. 2023, JATIS, 9, 014004
Li, X., Song, Y., Uitenbroek, H., et al. 2021, A&A, 646, A79
Liu, H., Jin, Z., Xiang, Y., & Ji, K. 2022, RAA, 22, 095005
Moran, T., Deming, D., Jennings, D. E., & McCabe, G. 2000, ApJ, 533, 1035
Moran, T. G., Jennings, D. E., Deming, L. D., et al. 2007, SoPh, 241, 213
Penn, M., Krucker, S., Hudson, H., et al. 2016, ApJL, 819, L30
Rimmele, T. R., Warner, M., Keil, S. L., et al. 2020, SoPh, 295, 172
Schad, T. A., Petrie, G., Kuhn, J., et al. 2024, SciA, 10, eadq1604
Schmidt, W., von der Lühe, O., Volkmer, R., et al. 2012, in ASP Conf. Ser. 463, Second ATST-EAST Meeting: Magnetic Fields from the Photosphere to the Corona, ed. T. R. Rimmele et al. (San Francisco, CA: ASP), 365
Shen, Y., Kewei, E., Fu, X., et al. 2022, ApOpt, 61, 5646
Simões, P. J. A., Kerr, G. S., Fletcher, L., et al. 2017, A&A, 605, A125
Unno, W. 1956, PASJ, 8, 108
Wang, Y., Feng, Z., Bai, X., et al. 2022, AR&T, 19, 125
Yang, X., Cao, W., Gorceix, N., et al. 2020, Proc. SPIE, 11447, 11447AG